



Article

Gem amphiboles from Mogok, Myanmar: crystal-structure refinement, infrared spectroscopy and short-range order–disorder in gem pargasite and fluoro-pargasite

Maxwell C. Day¹, Frank C. Hawthorne^{1*}, Umberto Susta², Giancarlo Della Ventura² and George E. Harlow³

¹Department of Geological Sciences, University of Manitoba, Winnipeg, Manitoba R3T 2N2, Canada; ²Dipartimento di Scienze, Università di Roma Tre, Largo S. Leonardo Murialdo 1, 00146 Rome, Italy; and ³Department of Earth and Planetary Sciences, American Museum of Natural History, Central Park West at 79th Street, New York, New York 10024-5192, USA

Abstract

The crystal structures of six gem-quality pargasites and fluoro-pargasites from Mogok, Myanmar, space group $C2/m$, $Z = 2$, have been refined to R_1 indices of 2.20–2.90% using $MoK\alpha$ X-radiation. The unit formulae were calculated from the results of electron-microprobe analysis, and were used with the refined site-scattering values and the observed mean bond lengths to assign site populations. T Al occurs at both the $T(1)$ and $T(2)$ sites but is strongly ordered at $T(1)$. ^{6}Al is partly disordered over the $M(2)$ and $M(3)$ sites but does not occur at the $M(1)$ site. 4Na is split between the $A(2)$ and $A(m)$ sites and K occurs at the $A(m)$ site. The infrared spectra in the principal OH-stretching region were measured and the fine structure was fit to component bands. The component bands were assigned to short-range ion arrangements over the configuration symbol $M(1)M(1)M(3)-O(3)-A-O(3):T(1)T(1)$ using the refined site-populations and the expected frequencies from previously assigned spectra in more simple amphibole compositions, and correspond to the local arrangements: (1) MgMgMg–OH–Na–OH:SiAl; (2) MgMgMg–OH–Na–F:SiAl; (3) MgMgAl–OH–Na–OH:SiAl and (4) MgMgAl–OH–Na–F:SiAl.

Keywords: pargasite, amphibole, gem, crystal structure, infrared spectroscopy, Myanmar, short-range order

(Received 11 April 2018; accepted 3 August 2018; Accepted Manuscript online: 14 September 2018; Associate Editor: Peter Leverett)

Introduction

Short-range order–disorder (SR-OD) is extremely common in amphiboles and describes the probability that local atomic arrangements occur more or less frequently than would be predicted by a random distribution of ions in the structure (Hawthorne and Della Ventura, 2007; Hawthorne *et al.*, 2005). However, SR-OD does not obey translational symmetry and spectroscopic methods are generally required to derive such information. The intensity and position of bands in infrared spectra are dependent upon the OH-stretching frequency, which is sensitive to the local arrangement of all cations in the structure (Hawthorne and Della Ventura, 2007). Consequently, the interpretation of such spectra may reveal the preference of cations to form specific local arrangements within the $C2/m$ amphibole structure (e.g. Hawthorne *et al.*, 1996a; Della Ventura *et al.*, 2014; Leissner *et al.*, 2015). The local version of bond-valence theory (Hawthorne, 1997) may also be used to constrain local arrangements of ions, and a combination of crystal-structure refinement, infrared or magic-angle spinning nuclear magnetic resonance (MAS NMR) spectroscopy, and local bond-valence

calculations can derive information on SR-OD in amphiboles provided that the composition of the amphibole is not overly complicated. The chemical variability of natural amphiboles gives rise to many overlapping absorption bands in the principal OH-stretching region of the infrared spectrum, and the spectra commonly do not contain enough information to allow the spectra to be fit correctly. This problem may be overcome by using (1) synthetic amphiboles (Raudsepp *et al.*, 1987a,b, 1991; Boschmann *et al.*, 1994; Della Ventura *et al.*, 1996a,b, 1997, 1998a,b, 1999, 2001, 2003; Hawthorne *et al.*, 1997, 2000; Robert *et al.*, 1999, 2000; Najorka and Gottschalk, 2003), the compositions of which are usually sufficiently constrained that a combination of Rietveld refinement or single-crystal refinement, infrared and MAS NMR spectroscopy, and local bond-valence arguments are sufficient to derive short-range order arrangements, or by using (2) gem amphiboles (Tait *et al.*, 2001; Abdu and Hawthorne, 2009; Heavyssege *et al.*, 2015) for which the compositions are commonly simple. Thus the majority of work on SR-OD in amphiboles involves interpretation of the spectra of synthetic and gem-quality samples where the composition either can be controlled or is simple enough to result in spectra that can be interpreted rigorously. In this study, we examine a series of gem-quality pargasites and fluoro-pargasites (Hawthorne *et al.*, 2012) by single-crystal structure refinement, infrared spectroscopy and electron-microprobe analysis in order to characterise their local arrangements.

*Author for correspondence: Frank C. Hawthorne, Email: frank_hawthorne@umanitoba.ca
Cite this article: Day M.C., Hawthorne F.C., Susta U., Della Ventura G. and Harlow G.E. (2019) Gem amphiboles from Mogok, Myanmar: crystal-structure refinement, infrared spectroscopy and short-range order–disorder in gem pargasite and fluoro-pargasite. *Mineralogical Magazine* 83, 361–371. <https://doi.org/10.1180/mgm.2018.149>

Table 1. Structure-refinement information for gem amphiboles from Mogok, Myanmar.

	AM1	AM2	AM3	AM6	AM7	AM8
<i>a</i> (Å)	9.845(5)	9.851(5)	9.881(7)	9.891(6)	9.887(6)	9.849(6)
<i>b</i>	17.940(10)	17.878(10)	17.976(12)	17.946(10)	17.956(11)	17.884(12)
<i>c</i>	5.294(3)	5.312(3)	5.295(3)	5.313(3)	5.306(3)	5.315(3)
β (°)	105.221(7)	105.373(12)	105.375(6)	105.456(8)	105.394(5)	105.345(9)
<i>V</i> (Å ³)	902.2(9)	902.1(9)	906.8(1)	909.0(9)	908.2(9)	902.8(1)
<i>Z</i>	2	2	2	2	2	2
Crystal size (µm)	40 × 40 × 100	15 × 40 × 100	40 × 60 × 110	40 × 40 × 80	60 × 80 × 140	60 × 80 × 100
Crystal colour	brown	yellow	green-tan	pale green	green-tan	light green
Radiation	MoK α	MoK α	MoK α	MoK α	MoK α	MoK α
Total reflections	16,315	16,324	16,339	16,441	16,363	16,340
Reflections in Ewald sphere	5297	5305	5324	5351	5342	5318
Unique reflections	1372	1372	1377	1387	1386	1379
<i>R</i> ₁ %	2.20	2.41	2.78	2.24	2.90	2.52
<i>R</i> (int)%	1.29	1.15	1.16	1.07	1.65	1.21
<i>wR</i> %	6.01	6.51	6.74	6.19	7.34	6.54
GoF	0.836	0.789	0.795	0.791	0.864	0.803

Experimental

Samples AM1, AM7 and AM8 are from the mineral collection of the U.S. National Museum of Natural History and have the catalogue numbers USNM 109256, USNM 108917 and USNM 108413, respectively. Samples AM2, AM3 and AM6 were supplied by Dudley Blowett of Mountain Minerals, Colorado. Single-crystal structure refinement (SREF), electron microprobe analysis (EMPA) and Fourier-transform infrared spectroscopy (FTIR) were done at the Department of Geological Sciences, University of Manitoba. Each sample was chosen for crystal clarity and uniform extinction under cross-polarised light. In preparation for SREF, crystals were cut to an approximate size-range 15–60 × 40–80 × 100–140 (µm) and attached to tapered glass fibres; similar samples were double-polished for FTIR analysis. In preparation for EMPA, the samples were mounted in epoxy in an acrylic ring, ground, polished and carbon coated.

Single-crystal X-ray diffraction (SREF)

Crystals were mounted on a Bruker D8 three-circle diffractometer equipped with a rotating-anode generator producing monochromatic MoK α X-radiation, multilayer optics and an APEX-II CCD detector. Totals of ~16,300 intensities were collected to 60°2 θ using 2–4 s per 0.2° frame with a crystal-to-detector distance of 5 cm. Empirical absorption corrections (SADABS, Sheldrick, 2008) were applied. Equivalent reflections were merged, resulting in ~5,320 reflections in the Ewald sphere. Intensities were averaged in the space group *C2/m*, resulting in ~1,370 unique reflections, and the intensities were reduced to structure factors. Unit-cell dimensions were obtained by least-squares refinement of the positions of ~4,000 reflections with $I > 10\sigma I$ and are given in Table 1. Each structure was refined in the space group *C2/m* with the *SHELXTL* version 6.14 program (Bruker AXS) to average *R*₁ indices of ~1.23% with anisotropic-displacement parameters at all sites. Atom positions and *U*_{eq} values are given in Table 2 and anisotropic-displacement parameters (Table S1) and crystallographic information files have been deposited with the Principal Editor of *Mineralogical Magazine* and are available as Supplementary material (see below). Selected interatomic distances are given in Table 3.

Electron microprobe analysis (EMPA)

Chemical analysis was done using a Cameca SX-100 electron microprobe operating in wavelength-dispersive mode using a voltage of

15 kV, a beam current of 20 nA, and a beam size of 1 µm. The following standards were used for K α lines: albite (Na); diopside (Si and Ca); fluoro-riebeckite (F); forsterite (Mg); andalusite (Al); orthoclase (K); titanite (Ti); fayalite (Fe); spessartine (Mn); tugtupite (Cl); VP₂O₇ (V); chromite (Cr); and gahnite (Zn). Ten analytical points were measured on each sample. Data were corrected using the *PAP* procedure of Pouchou and Pichoir (1985), and the mean compositions are given in Table 4, together with the unit formulae calculated on the basis of (O,OH,F,Cl) = 24 atoms per formula unit (apfu) with (OH,F,Cl) = 2 apfu.

Infrared spectroscopy

Fourier-transform infrared (FTIR) spectra in the principal OH-stretching region were collected for all gem amphibole samples using a Bruker Tensor 27 FTIR spectrometer equipped with a KBr beam splitter and a DLATGS detector. It should be noted that the spectra of AM6 and AM7 contain relatively more noise due to lack of material.

Spectra over the range 4000–400 cm⁻¹ were collected by averaging 100 scans at an operating resolution of 4 cm⁻¹. Base-line corrections were done using the *OPUS* software (Bruker AXS) and spectra analysis in the 3800–3600 cm⁻¹ range was done using the *OMNIC* software (Thermo Scientific™). Spectra were fit using Gaussian curves of similar width (full-width-at-half-maximum) with the program *FITYK V0.9.8* (Wojdyr, 2010).

The *C2/m* amphibole structure

The general formula for the amphiboles can be written as A_{0–1}B₂C₅T₈O₂₂W₂, where A = Na, K, Ca, Li; B = Na, Li, Ca, Mn²⁺, Fe²⁺, Mg, Sr; C = Mg, Fe²⁺, Mn²⁺, Al, Fe³⁺, Mn³⁺, Ti⁴⁺, Li; T = Si, Al, Ti⁴⁺; W = (OH), F, Cl, O²⁻. The *C2/m* amphibole structure is shown in Fig. 1 and the correspondence between the general formula and the sites may be written as follows: ^A[A(2), A(*m*)]^BM(4)₂^C[M(1)₂M(2)₂M(3)]^T[T(1)₄T(2)₄]O₂₂^WO(3)₂. A detailed summary of previous work on the structure and crystal chemistry of amphiboles was given by Hawthorne (1981, 1983a), Hawthorne and Oberti (2007) and Oberti *et al.* (2007).

Long-range site-populations

The *T* sites

These amphiboles contain 1.79–2.41 apfu Al at the *T* sites (Table 4). The scattering values of Si and Al are similar, which

Table 2. Atom coordinates and equivalent-displacement parameters (\AA^2) for gem amphiboles from Mogok, Myanmar.

Site	AM1				AM2				AM3			
	x	y	z	$U_{\text{eq/iso}}$	x	y	z	$U_{\text{eq/iso}}$	x	y	z	$U_{\text{eq/iso}}$
T(1)	0.28098(3)	0.08540(2)	0.30277(6)	0.00864(11)	0.27947(4)	0.08658(2)	0.30493(8)	0.00787(11)	0.28071(4)	0.08528(2)	0.30323(7)	0.00838(12)
T(2)	0.29054(3)	0.17336(2)	0.81335(6)	0.00694(11)	0.29135(4)	0.17451(2)	0.81851(7)	0.00623(11)	0.29042(4)	0.17331(2)	0.81328(7)	0.00672(12)
M(1)	0	0.08901(3)	1/2	0.00832(19)	0	0.09004(4)	1/2	0.0074(2)	0	0.08908(4)	1/2	0.0078(2)
M(2)	0	0.17608(3)	0	0.00583(19)	0	0.17608(3)	0	0.0041(2)	0	0.17566(3)	0	0.0053(2)
M(3)	0	0	0	0.0076(3)	0	0	0	0.0066(3)	0	0	0	0.0072(3)
M(4)	0	0.27972(2)	1/2	0.01099(13)	0	0.28086(2)	1/2	0.00915(13)	0	0.27986(2)	1/2	0.01039(14)
A(2)	0	0.4769(3)	0	0.034(2)	0	0.4838(3)	0	0.0216(16)	0	0.4728(5)	0	0.028(2)
A(m)	0.5436(6)	0	0.0927(13)	0.0366(18)	0.53789(8)	0	0.0797(17)	0.021(2)	0.5343(9)	0	0.0753(19)	0.038(3)
O(1)	0.10658(9)	0.08739(5)	0.21576(17)	0.01039(19)	0.10371(11)	0.09034(6)	0.2125(2)	0.0095(2)	0.10642(10)	0.08696(6)	0.21631(19)	0.0099(2)
O(2)	0.11892(9)	0.17252(5)	0.73374(17)	0.00915(18)	0.11812(11)	0.17430(6)	0.7413(2)	0.0084(2)	0.11931(10)	0.17290(5)	0.73195(19)	0.0085(2)
O(3)	0.10684(12)	0	0.7149(2)	0.0107(3)	0.10730(15)	0	0.7141(3)	0.0095(4)	0.10750(14)	0	0.7169(3)	0.0108(4)
O(4)	0.36645(10)	0.25111(5)	0.79068(17)	0.01097(19)	0.36965(11)	0.25268(6)	0.7934(2)	0.0099(2)	0.36663(11)	0.25065(6)	0.78889(19)	0.0105(2)
O(5)	0.35124(9)	0.14003(6)	0.11149(17)	0.01221(19)	0.35277(11)	0.14174(6)	0.1176(2)	0.0104(2)	0.35047(10)	0.14083(6)	0.11322(19)	0.0114(2)
O(6)	0.34469(9)	0.11685(5)	0.61002(18)	0.01210(19)	0.34296(11)	0.11751(6)	0.6142(2)	0.0112(2)	0.34472(10)	0.11625(6)	0.6124(2)	0.0121(2)
O(7)	0.34234(14)	0	0.2782(3)	0.0136(3)	0.33758(17)	0	0.2782(3)	0.0139(3)	0.34214(16)	0	0.2752(3)	0.0133(3)

Site	AM6				AM7				AM8			
	x	y	z	$U_{\text{eq/iso}}$	x	y	z	$U_{\text{eq/iso}}$	x	y	z	$U_{\text{eq/iso}}$
T(1)	0.27909(4)	0.08612(2)	0.30529(7)	0.00812(10)	0.27907(4)	0.08597(2)	0.30456(8)	0.00842(13)	0.27992(4)	0.08646(2)	0.30489(7)	0.00863(12)
T(2)	0.29065(4)	0.17399(2)	0.81676(7)	0.00663(10)	0.29038(4)	0.17390(2)	0.81518(7)	0.00677(13)	0.29143(4)	0.17444(2)	0.81855(7)	0.00708(12)
M(1)	0	0.08969(4)	1/2	0.0077(2)	0	0.08948(4)	1/2	0.0086(2)	0	0.08991(4)	1/2	0.0083(2)
M(2)	0	0.17609(3)	0	0.00477(19)	0	0.17604(4)	0	0.0057(2)	0	0.17608(3)	0	0.0047(2)
M(3)	0	0	0	0.0076(3)	0	0	0	0.0077(3)	0	0	0	0.0074(3)
M(4)	0	0.28064(2)	1/2	0.00949(12)	0	0.28018(2)	1/2	0.01024(15)	0	0.28086(2)	1/2	0.00995(14)
A(2)	0	0.4878(2)	0	0.0059(16)	0	0.4875(2)	0	0.0090(16)	0	0.4809(3)	0	0.0294(17)
A(m)	0.5363(6)	0	0.0743(11)	0.0204(12)	0.5374(6)	0	0.0767(12)	0.0194(15)	0.5379(9)	0	0.0805(19)	0.025(2)
O(1)	0.10448(10)	0.08913(6)	0.21492(19)	0.0097(2)	0.10487(11)	0.08861(6)	0.2156(2)	0.0102(2)	0.10402(11)	0.09017(6)	0.2124(2)	0.0100(2)
O(2)	0.11842(10)	0.17378(5)	0.73711(19)	0.00862(19)	0.11900(11)	0.17359(6)	0.7351(2)	0.0089(2)	0.11801(11)	0.17418(6)	0.7411(2)	0.0092(2)
O(3)	0.10634(14)	0	0.7146(2)	0.0096(4)	0.10711(16)	0	0.7151(3)	0.0109(4)	0.10737(14)	0	0.7140(3)	0.0102(4)
O(4)	0.36824(11)	0.25181(6)	0.79307(19)	0.0107(2)	0.36742(12)	0.25134(6)	0.7923(2)	0.0111(2)	0.36963(11)	0.25269(6)	0.7931(2)	0.0106(2)
O(5)	0.35096(10)	0.14074(6)	0.11572(19)	0.0111(2)	0.35041(11)	0.14023(7)	0.1135(2)	0.0115(2)	0.35295(11)	0.14195(6)	0.11809(19)	0.0111(2)
O(6)	0.34365(10)	0.11791(6)	0.61223(19)	0.0117(2)	0.34387(11)	0.11779(7)	0.6116(2)	0.0121(2)	0.34307(11)	0.11727(6)	0.6141(2)	0.0120(2)
O(7)	0.33793(16)	0	0.2848(3)	0.0143(3)	0.33855(18)	0	0.2847(3)	0.0150(3)	0.33826(16)	0	0.2766(3)	0.0143(3)

precludes accurate derivation of site populations by site-scattering refinement (Hawthorne, 1983c; Hawthorne *et al.*, 1995). However, the difference in ionic radii of ${}^T\text{Si}$ (0.26 Å) and ${}^T\text{Al}$ (0.39 Å) (Shannon, 1976) allows derivation of site populations from $\langle T-O \rangle$ distances (e.g. Papike *et al.*, 1969, Hawthorne and Grundy, 1973a,b, 1977; Robinson *et al.*, 1973; Bocchio *et al.*, 1978; Hawthorne, 1981, 1983a,b; Oberti *et al.*, 1995a). The preference of ${}^T\text{Al}$ for $T(1)$ was confirmed by neutron diffraction (Welch and Knight, 1999) and by spectroscopic methods (Welch *et al.*, 1994, 1998; Jenkins *et al.*, 1997; Najorka and Gottschalk, 2003; Della Ventura *et al.*, 2007). Hawthorne and Oberti (2007) showed that grand $\langle T-O \rangle$ distances are also influenced by inductive effects where ${}^T\text{Al} < 0.50$ apfu, but vary linearly with ${}^T\text{Al}$ content where ${}^T\text{Al} > 0.50$ apfu. As shown in Fig. 2a, these gem amphiboles accord very closely with this relation with deviations of < 0.001 Å. Hawthorne and Oberti (2007) also gave predictive relations for the Al site populations of the $T(1)$ and $T(2)$ sites based on the observed $\langle T(1)-O \rangle$ and $\langle T(2)-O \rangle$ distances which were used here to derive site populations for the $T(1)$ and $T(2)$ sites. The resulting site-populations are in accord with the ${}^T\text{Al}$ contents derived by electron-microprobe analysis (Fig. 2b).

The $M(1,2,3)$ sites

The total refined scattering at the $M(1,2,3)$ sites (62.95–63.97 electrons per formula unit [epfu]) (Table 5) shows an extremely small range which is consistent with the C-group cations indicated by the unit formulae of Table 4 (Fig. 3a). Similarly, the variation in grand $\langle M(1,2,3)-O \rangle$ distances shows a linear correlation with

the mean radius (r) of the C-group cations from the unit formula in Table 4 (Fig. 3b). The compositions of the C group are dominated by Mg (3.59–4.14 apfu) and Al (0.56–1.28 apfu), and the similarity of the scattering factors of Mg and Al ensure the very narrow range of refined site-scattering from the $M(1,2,3)$ sites. The net refined site-scattering values at $M(1,2,3)$ deviate from the effective scattering from the C-group cations of the unit formulae (Table 4) by an average of 0.31 epfu. To facilitate assignment of site populations from the refined site-scattering values, the latter were adjusted (generally within one standard deviation, Table 5) to conform to the effective scattering from the C-group cations of the unit formulae indicated by the chemical formulae.

In most amphiboles, ${}^{[6]}\text{Al}$ is ordered at $M(2)$ (e.g. Hawthorne, 1981, 1983a; Oberti *et al.*, 2007). However, Semet (1973) showed by infrared spectroscopy that ${}^{[6]}\text{M}^{3+}$ cations disorder over the $M(2)$ and $M(1)$ and/or $M(3)$ sites in Mg-rich synthetic amphiboles, and Raudsepp *et al.* (1987a,b, 1991) showed by infrared spectroscopy and Rietveld refinement that this disorder occurs over the $M(2)$ and $M(3)$ sites. Oberti *et al.* (1995b) showed the same disorder of ${}^{[6]}\text{Al}$ over the $M(2)$ and $M(3)$ sites in Mg-rich pargasites from peridotites, and this disorder of ${}^{[6]}\text{Al}$ over the $M(2)$ and $M(3)$ has since been shown to be the case for Mg-rich synthetic (e.g. Welch and Knight, 1999) and natural amphiboles (e.g. Tait *et al.*, 2001; Heavysage *et al.*, 2015). The absence of Al at the $M(1)$ site allows us to calculate the $M(1)$ site-populations directly from the refined site-scattering values (Table 5) using the scattering curves for Mg and the dominant transition metal in the unit formulae. The resultant site-populations are also given in Table 5.

Table 3. Interatomic distances (Å) for gem amphiboles from Mogok, Myanmar.

	AM1	AM2	AM3	AM6	AM7	AM8
T(1)–O(1)	1.6571(13)	1.6711(14)	1.6608(16)	1.6657(15)	1.6613(15)	1.6723(15)
T(1)–O(5)	1.6829(11)	1.6926(13)	1.6889(13)	1.6917(12)	1.6896(13)	1.6929(13)
T(1)–O(6)	1.6799(13)	1.6883(14)	1.6855(13)	1.6845(13)	1.6842(14)	1.6888(14)
T(1)–O(7)	1.6645(10)	1.6693(11)	1.6698(12)	1.6652(11)	1.6652(12)	1.6701(12)
<T(1)–O>	1.6711(12)	1.6803(14)	1.6763(14)	1.6768(13)	1.6751(14)	1.6810(14)
T(2)–O(2)	1.6306(13)	1.6460(14)	1.6304(16)	1.6422(14)	1.6339(15)	1.6476(15)
T(2)–O(4)	1.6016(12)	1.6188(13)	1.6026(14)	1.6145(13)	1.6053(14)	1.6202(14)
T(2)–O(5)a	1.6464(12)	1.6505(14)	1.6479(13)	1.6523(13)	1.6504(14)	1.6519(13)
T(2)–O(6)	1.6650(11)	1.6637(13)	1.6655(13)	1.6650(12)	1.6629(13)	1.6661(13)
<T(2)–O>	1.6359(12)	1.6448(14)	1.6366(14)	1.6435(13)	1.6381(14)	1.6465(14)
M(1)–O(1)	2.0483(12)	2.0501(14)	2.0497(13)	2.0485(13)	2.0454(14)	2.0528(13)
M(1)–O(1)d	2.0483(12)	2.0501(14)	2.0497(13)	2.0485(13)	2.0454(14)	2.0528(13)
M(1)–O(2)	2.0942(12)	2.1154(13)	2.0978(14)	2.1094(13)	2.1076(14)	2.1157(14)
M(1)–O(2)d	2.0942(12)	2.1154(14)	2.0978(14)	2.1094(13)	2.1076(14)	2.1156(14)
M(1)–O(3)	2.0789(11)	2.0891(13)	2.0891(13)	2.0876(12)	2.0891(14)	2.0883(13)
M(1)–O(3)e	2.0790(11)	2.0891(13)	2.0891(13)	2.0876(12)	2.0891(13)	2.0883(13)
<M(1)–O>	2.0738(12)	2.0849(14)	2.0789(13)	2.0818(13)	2.0807(14)	2.0856(13)
M(2)–O(1)	2.0755(13)	2.0141(14)	2.0789(14)	2.0442(13)	2.0538(15)	2.0181(14)
M(2)–O(1)f	2.0755(13)	2.0141(14)	2.0789(14)	2.0441(13)	2.0538(15)	2.0181(14)
M(2)–O(2)b x2	2.0563(12)	2.0228(13)	2.0722(14)	2.0486(13)	2.0589(14)	2.0228(13)
M(2)–O(4)c x2	1.9744(12)	1.9309(13)	1.9899(13)	1.9538(13)	1.9663(14)	1.9321(13)
<M(2)–O>	2.0354(13)	1.9892(14)	2.0470(14)	2.0155(13)	2.0263(15)	1.9910(14)
M(3)–O(1)g x3	2.0578(12)	2.0773(13)	2.0548(13)	2.0739(12)	2.0702(14)	2.0768(14)
M(3)–O(1)	2.0578(12)	2.0773(13)	2.0548(13)	2.0739(12)	2.0702(14)	2.0768(14)
M(3)–O(3)b x2	2.0539(14)	2.0678(17)	2.0543(16)	2.0629(16)	2.0631(17)	2.0688(16)
<M(3)–O>	2.0565(13)	2.0741(14)	2.0546(14)	2.0702(13)	2.0678(15)	2.0741(15)
M4–O(2)	2.4165(13)	2.4156(14)	2.4140(15)	2.4187(14)	2.4135(15)	2.4176(15)
M4–O(2)d	2.4165(13)	2.4156(14)	2.4140(15)	2.4187(14)	2.4135(15)	2.4176(15)
M4–O(4)c x2	2.3377(12)	2.3447(14)	2.3338(14)	2.3545(14)	2.3502(14)	2.3440(14)
M4–O(5)c x2	2.6204(13)	2.5656(14)	2.6087(14)	2.5939(14)	2.6126(15)	2.5627(14)
M4–O(6)c x2	2.5667(14)	2.5612(15)	2.5845(16)	2.5600(15)	2.5642(16)	2.5637(16)
<M4–O>	2.4853(13)	2.4718(14)	2.4853(15)	2.4818(14)	2.4851(15)	2.4720(15)
A(m)–O(6)i x2	2.6780(48)	2.7247(65)	2.7352(72)	2.7579(46)	2.7487(49)	2.7200(71)
A(m)–O(7)	2.4314(45)	2.4720(50)	2.4069(60)	2.5042(35)	2.4969(40)	2.4570(54)
A(m)–O(7)h	2.5050(48)	2.5212(54)	2.4772(63)	2.5402(36)	2.5357(41)	2.5128(57)
<A(m)–O>	2.5731(47)	2.6107(59)	2.5886(67)	2.6401(41)	2.6325(45)	2.6025(63)
A(2)–O(5)j x2	2.7106(50)	2.8303(39)	2.6803(75)	2.8902(35)	2.8774(36)	2.7929(48)
A(2)–O(6)c x2	2.7877(39)	2.8623(32)	2.7311(58)	2.9214(29)	2.9177(31)	2.8284(39)
A(2)–O(7)j x2	2.4394(20)	2.4664(20)	2.4498(27)	2.4900(19)	2.4820(21)	2.4605(20)
<A(2)–O>	2.6459(36)	2.7197(24)	2.6204(53)	2.7672(28)	2.7590(29)	2.6939(36)

Symmetry codes: a: $x, y, z+1$; b: $x, y, z-1$; c: $-x+1/2, -y+1/2, -z+1$; d: $-x, y, -z+1$; e: $-x, -y, -z+1$; f: $-x, y, -z$; g: $-x, -y, -z$; h: $-x+1, -y, -z$; i: $-x+1, -y, -z+1$.

Preliminary site-populations for the $M(2)$ and $M(3)$ sites were calculated from the refined site-scattering values (Table 5) in terms of Mg^* ($= Mg + Al$) and the dominant transition metal. The results indicate that all V^{3+} , Cr^{3+} and Ti^{4+} occurs at the $M(2)$ site and the $\langle M(2)–O \rangle$ bond lengths are in accord with this assignment. The X-ray scattering factors of Mg ($Z = 12$) and Al ($Z = 13$) are very close, and mean bond lengths must be used to assign $^{[6]}Al$ and $^{[6]}Mg$ as the sizes of $^{[6]}Mg$ ($r = 0.72$ Å) and $^{[6]}Al$ ($r = 0.535$ Å) are significantly different (Shannon, 1976). There are equations relating $\langle M(2)–O \rangle$ and $\langle M(3)–O \rangle$ distances to constituent cation and anion radii and to other stereochemical aspects of the adjacent sites (Hawthorne and Oberti, 2007). Using these equations, $^{[6]}Al$ and $^{[6]}Mg$ were assigned to $M(2)$ and $M(3)$ such that there is an equally good fit between the observed and calculated $\langle M(2)–O \rangle$ and $\langle M(3)–O \rangle$ values; the deviations are within the error of estimate for each site given by Hawthorne and Oberti (2007). The resultant site-populations are given in Table 5.

The $M(4)$ site

The unit formulae (Table 4) indicate that the $M(4)$ site is occupied dominantly by Ca with minor Na , and the refined site-scattering values are in accord with this occupancy (Table 5). Thus the site populations were assigned directly from the formulae of Table 4.

The A site

In accord with previous work on local order–disorder in the A cavity of monoclinic amphiboles (e.g. Hawthorne and Grundy, 1972, 1973a,b; Hawthorne *et al.*, 1996b), Na was assigned to the $A(2)$ site and ($Na + K$) was assigned to the $A(m)$ site in agreement with the refined site-scattering values at these sites (Table 5) and the formulae derived from electron-microprobe analysis (Table 4).

Short-range order in the $C2/m$ amphibole structure

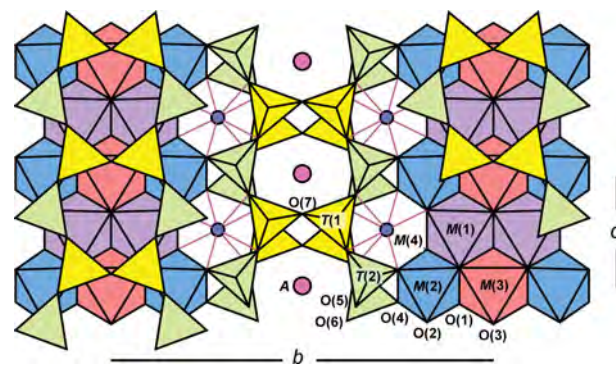
The infrared spectra of amphiboles are strongly affected by short-range order (SRO): the occurrence of local clusters of ions that may

Table 4. Chemical composition (wt.%) and unit formula (apfu) for gem amphiboles from Mogok, Myanmar.

	AM1	AM2	AM3	AM6	AM7	AM8
Wt.%						
SiO ₂	44.29	40.20	43.66	41.00	42.60	39.82
Al ₂ O ₃	15.22	22.04	14.85	18.43	16.72	22.18
TiO ₂	1.03	0.45	0.48	1.23	0.76	0.74
FeO	1.14	0.37	0.34	0.42	0.77	0.23
MgO	19.02	17.35	19.85	18.98	19.11	17.14
CaO	12.55	12.79	13.27	13.33	13.03	12.90
Na ₂ O	4.02	3.12	3.38	2.08	2.27	3.37
K ₂ O	0.38	1.48	0.32	2.50	2.40	1.08
F	2.29	1.69	1.31	2.60	2.06	1.63
MnO	0.03	0.01	0.01	0	0.03	0.00
Cl	0.01	0.01	0.07	0.02	0.10	0.01
V ₂ O ₃	0.03	0.06	1.91	0.04	0.03	0.16
Cr ₂ O ₃	0.01	0.03	0.08	0.12	0.02	0.22
ZnO	0.04	0.03	0.02	0.01	0.02	0.02
H ₂ O	1.05	1.34	1.52	0.89	1.15	1.36
O = F	-0.96	-0.71	-0.55	-1.09	-0.87	-0.69
Total	100.15	100.26	100.52	100.56	100.20	100.18
Atoms per formula unit						
Si	6.21	5.64	6.11	5.78	6.02	5.59
Al	1.79	2.36	1.89	2.22	1.98	2.41
ΣT	8.00	8.00	8.00	8.00	8.00	8.00
Al ³⁺	0.73	1.28	0.56	0.84	0.80	1.26
Ti ⁴⁺	0.11	0.05	0.05	0.13	0.08	0.08
V ³⁺	0	0.01	0.21	0.01	0	0.02
Cr ²⁺	0	0	0.01	0.01	0	0.02
Fe ²⁺	0.13	0.04	0.04	0.05	0.09	0.03
Mg ²⁺	3.98	3.63	4.14	3.99	4.02	3.59
ΣC	4.95	5.01	5.01	5.03	4.99	5.00
Ca ²⁺	1.89	1.92	1.99	2.00	1.97	1.94
Na ⁺	0.11	0.08	0.01	0.00	0.03	0.06
ΣB	2.00	2.00	2.00	2.00	2.00	2.00
Na ⁺	0.98	0.77	0.91	0.57	0.59	0.86
K ⁺	0.07	0.27	0.06	0.45	0.43	0.19
ΣA	1.05	1.04	0.97	1.02	1.02	1.05
OH	0.98	1.25	1.42	0.84	1.08	1.28
F	1.02	0.75	0.58	1.16	0.92	0.72
ΣO(3)	2	2	2	2	2	2

(or may not) give rise to discrete bands in the principal OH-stretching region of the infrared (Strens, 1966). Hawthorne *et al.* (1996a) showed that SRO is common in amphiboles, and that bands in the infrared can be assigned to specific local clusters of ions that centre on the O(3) site (Hawthorne and Grundy, 1976). Extensive work since then (Hawthorne *et al.*, 1997, 2000; Della Ventura *et al.*, 1999, 2001, 2003; Robert *et al.*, 1999, 2000; Hawthorne and Della Ventura, 2007; Leissner *et al.*, 2015) has shown that both nearest-neighbour (NN) and next-nearest-neighbour (NNN) cations affect the principal OH-stretching frequency of the locally associated (OH) group, and both infrared and Raman spectroscopy of the principal OH-stretching region may be used as a sensitive probe of NN and NNN short-range arrangements in amphiboles.

The arrangement of atoms around the O(3) site in the C₂/m amphibole structure is shown in Fig. 4. The O(3) site is situated at the centre of the strip of octahedra and is bonded to two M(1) and one M(3) cations. Hawthorne and Grundy (1976) found that where O(3) = (OH), the H atom is ~ 1 Å (0.957(6) Å) away from the O(3) site and that the H atom forms a hydrogen bond with one of the O(7) oxygen atoms, shown by the dashed black line in Fig. 4. The strength of the O(3)–H bond controls the frequency of the principal OH-stretching vibration which is in turn related to the strength of the H...O(7) hydrogen bond (Hawthorne *et al.*, 2005). It follows that any variation in the occupancy of

**Fig. 1.** The monoclinic C₂/m amphibole structure viewed along 001.

the sites locally associated with the O(3) and O(7) sites gives rise to fine structure in the principal OH-stretching region of the infrared. Such locally associated sites include the NN M(1)M(1)M(3), T(1)T(1) and A(2)/m sites. The M(1)M(1)M(3) sites are locally associated with the O⁽³⁾(OH) group which also interacts with the cation occupying the A site. Satisfaction of the bond-valence requirements at the O(7) site also influences the strength of the locally associated hydrogen bond and is controlled by the occupancy of the locally associated T(1) sites.

The configuration symbol and possible arrangements

Hawthorne *et al.* (2005) introduced the idea of a 'configuration symbol' which denotes the NN and NNN cation sites associated with the O(3) site: M(1)M(1)M(3)–O(3)–A:T(1)T(1)–M(2)M(2)M(3)–M(2)M(2). Della Ventura *et al.* (1999) showed that the major bands in the spectrum of pargasite are slightly split by different occupancy of NNN sites. However, this splitting is small, and Robert *et al.* (2000) ignored this splitting in fitting of the spectra of pargasite–fluoro-pargasite solid solutions. We use the same approach here, and consider only NN and NNN effects involving the configuration symbol M(1)M(1)M(3)–O(3)–A:T(1)T(1). However, we need to incorporate the NNN effect of F across the occupied A site into the configuration symbol (see below for a discussion of this effect). We shall do so in the following way: M(1)M(1)M(3)–O(3)–A–O(3):T(1)T(1) where the following arrangements about the A site are possible: M(1)M(1)M(3)–OH–A–OH:T(1)T(1); M(1)M(1)M(3)–OH–A–F:T(1)T(1); and M(1)M(1)M(3)–F–A–F:T(1)T(1); the last arrangement has no expression in the infrared.

Constraints of composition

(1) Inspection of Table 4 shows that the A-group cations completely occupy the A site, and hence local arrangements will involve only A = Na⁺ (Na⁺ = Na + K).

(2) For Mg-rich compositions, it has been shown both crystallographically (e.g. Raudsepp *et al.*, 1987a,b; Oberti *et al.*, 1995b; Welch and Knight, 1999) and spectroscopically (e.g. Semet, 1973; Raudsepp *et al.*, 1987b; Welch *et al.*, 1994, 1998; Della Ventura *et al.*, 1998b) that the trivalent C-group cations are partly disordered over the M(2) and M(3) sites, and Oberti *et al.* (1995b) showed how the <M(2)–O> and <M(3)–O> distances can be used to derive the site populations associated with this disorder. Using the site populations of the M(3) site (Table 5), we may calculate the relative

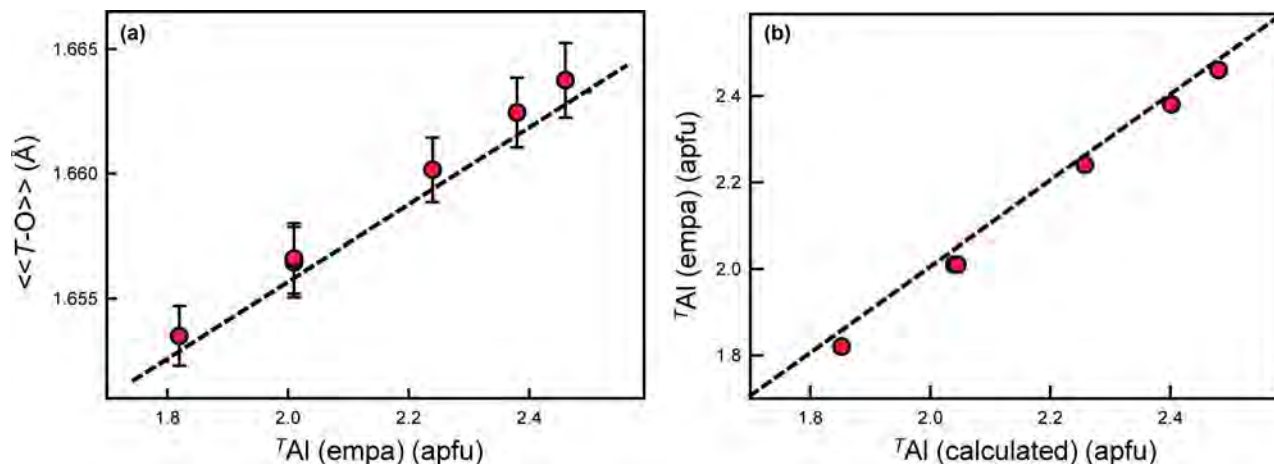


Fig. 2. (a) Grand $\langle T-O \rangle$ (Å) plotted against TAl (apfu) with associated error; and (b) calculated TAl (apfu) plotted against observed (EMPA) TAl (apfu) for each sample (shown as red dots). The dashed black line in (a) represents the equation given by Hawthorne and Oberti (2007), and in (b) the 1:1 relation between the variables.

amounts of local arrangements at $M(1)M(1)M(3)$ in the following manner: $MgMgMg:MgMgAl = {}^{M(3)}Mg^*:{}^{M(3)}Al$ ($Mg^* = Mg + Fe^{2+}$).

(3) Arrangements involving $T(1)-O(7)-T(1)$ are affected by the amount of TAl in the structure. Hawthorne and Oberti (2007) state that $T(1)Al-O(7)-T(1)Al$ arrangements do not occur unless O(7) is locally associated with Ca at the A site, as in fluorocannilloite (Hawthorne *et al.*, 1996b). This is not the case for any of the amphiboles examined here (Table 4), $T(1)Al-O(7)-T(1)Al$ arrangements cannot occur, and the site populations of Table 5 may be used to calculate the frequencies of occurrence of arrangements involving the $T(1)T(1)$ sites: $T(1)Al-O(7)-T(1)Si = T(1)Al/2$ and $T(1)Si-O(7)-T(1)Si = 1 - T(1)Al/2$.

(4) There is only minor occupancy of the C-group by divalent cations other than Mg (Fe^{2+}), and arrangements involving Fe^{2+} may be ignored (except perhaps for crystal AM1).

(5) Heavysege *et al.* (2015) proposed that arrangements involving $M(1)M(1)M(3) = MgMgAl$ should be locally associated with the arrangement $T(1)T(1) = SiAl$, as the bridging O(7) requires more bond valence from the hydrogen bond when linked to SiAl than when linked to SiSi. This local arrangement is possible as $T(1)Al > {}^{M(3)}Al$ in all amphiboles of Table 5.

The nearest-neighbour effect of F

There are three possible local arrangements involving $M(3)$ and OH,F: [1] OH- $M(3)$ -OH; [2] OH- $M(3)$ -F; and [3] F- $M(3)$ -F; these arrangements gives rise to two, one and zero absorption events in the infrared, respectively. Thus the proportion of absorption events to null-absorption events is equal to the (OH):F ratio.

There is no disorder of trivalent cations over $M(2)$ and $M(3)$ in amphiboles where O(3) is occupied by F (Raudsepp *et al.*, 1987b; Oberti *et al.*, 1995c, 1998). This means that in amphiboles where both (OH) and F are present in major amounts, F will be strongly to completely associated with the local arrangement $M(1)M(1)M(3) = MgMgMg$ and not with the local arrangement $MgMgAl$. Above (point 2)), we showed that the $T(1)T(1)$ arrangements occur in the ratio $T(1)Al/2:1 - T(1)Al/2$. Inspection of Table 5 shows that $T(1)Al/2 > {}^{M(3)}Al$ for all crystals examined here, in accord with this short-range constraint. In addition, the number of arrangements, $T(1)T(1) = SiSi = 1 - T(1)Al/2$, is always less than the amount of F in the amphibole, and hence all local arrangements

$MgMgMg-X-Na:SiSi$ will have $X = F$ and have no expression in the infrared. The local arrangement $MgMgMg-OH-Na:SiSi$ gives rise to a band at $3730-3740\text{ cm}^{-1}$ (Della Ventura *et al.*, 1999; Hawthorne, 2016). In accord with the above discussion, this band is not observed in the spectra of the amphiboles examined here (Fig. 5). A similar absence of this $3730-3740\text{ cm}^{-1}$ band occurs in the spectra of fluoro-edenite and fluoro-pargasite (Della Ventura *et al.*, 2014). In the Mogok amphiboles, the local arrangement $MgMgMg-OH-Na:SiAl$ gives rise to a band at $3720-3710\text{ cm}^{-1}$ ($\sim 3711\text{ cm}^{-1}$) as $T(1)Si$ substituted for by $T(1)Al$ results in a relative band displacement of -20 cm^{-1} (Della Ventura *et al.*, 1999; Hawthorne, 2016). The occurrence of such a band is in accord with the site populations of these amphiboles, and this is typically the highest-frequency band observed (Fig. 5, band A).

The next-nearest-neighbour effect of F

Infrared spectroscopy of amphiboles in the tremolite-fluoro-tremolite series show a single OH-stretching band at 3674 cm^{-1} (Jenkins, 1987; Gottschalk *et al.*, 1999; Robert *et al.*, 1999), and the position of this band does not change with varying F content (apfu). This 'one-mode behaviour' (Chang and Mitra, 1968) is due to a lack of coupling between O(3) sites adjacent across the A cavity, in accord with the fact that the A site in tremolite is vacant and cannot couple O(3) arrangements across the A-site cavity (Hawthorne *et al.*, 2005).

Amphibole with an occupied A site shows two-mode behaviour (Chang and Mitra, 1968) with regard to the variation in (OH) and F in the structure (Robert *et al.*, 1999, 2000). Work on the richterite-fluoro-richterite series shows three distinct bands in the infrared, one at 3730 cm^{-1} due to the arrangement $MgMgMg-OH-Na-OH:SiSi$, one at 3674 cm^{-1} due to the arrangement $MgMgMg-OH-\square-OH:SiSi$, and one at 3711 cm^{-1} due to the arrangement $MgMgMg-OH-Na-F:SiSi$ (Della Ventura *et al.*, 1998a, 1999; Hawthorne *et al.*, 2005). This 'two-mode behaviour' (Chang and Mitra, 1968) suggests that the local OH-group arrangement is affected by the adjacent arrangement involving F; the occurrence of an additional band in the richterite spectrum ($A = Na$) compared to the tremolite spectrum ($A = \square$) indicates that coupling of O(3) arrangements adjacent across the A cavity occurs only in the presence of an occupied A site. It should also be noted that the intensity of the band at

Table 5. Refined and calculated site-scattering (ss) values (epfu) and assigned site-populations (apfu) for gem amphiboles from Mogok, Myanmar.

Site	AM#	Assigned site population	Σ	Refined ss values	Calculated ss values	<bl> (Å)
T(1)	1	2.37 Si + 1.63 Al	4.00	–	–	1.671
	2	2.07 Si + 1.93 Al	4.00	–	–	1.680
	3	2.20 Si + 1.80 Al	4.00	–	–	1.676
	6	2.20 Si + 1.80 Al	4.00	–	–	1.676
	7	2.24 Si + 1.76 Al	4.00	–	–	1.675
	8	2.06 Si + 1.94 Al	4.00	–	–	1.681
T(2)	1	3.81 Si + 0.19 Al	4.00	–	–	1.636
	2	3.55 Si + 0.45 Al	4.00	–	–	1.645
	3	3.79 Si + 0.21 Al	4.00	–	–	1.637
	6	3.56 Si + 0.44 Al	4.00	–	–	1.644
	7	3.75 Si + 0.25 Al	4.00	–	–	1.638
	8	3.48 Si + 0.52 Al	4.00	–	–	1.647
M(1)	1	1.88 Mg + 0.12 Fe ²⁺	2.00	25.46(9)	25.68	2.074
	2	1.94 Mg + 0.06 Fe ²⁺	2.00	24.64(11)	24.84	2.085
	3	1.94 Mg + 0.06 Fe ²⁺	2.00	25.46(10)	24.84	2.079
	6	1.96 Mg + 0.04 Fe ²⁺	2.00	24.49(10)	24.56	2.082
	7	1.91 Mg + 0.09 Fe ²⁺	2.00	25.22(11)	25.26	2.081
	8	1.93 Mg + 0.07 Fe ²⁺	2.00	24.59(10)	24.98	2.086
M(2)	1	1.32 Mg + 0.56 Al + 0.11 Ti ⁴⁺ + 0.01 Fe ²⁺	2.00	25.70(9)	25.80	2.035
	2	0.68 Mg + 1.26 Al + 0.05 Ti ⁴⁺ + 0.01 V ³⁺	2.00	25.64(10)	25.87	1.989
	3	1.38 Mg + 0.36 Al + 0.05 Ti ⁴⁺ + 0.21 V ³⁺	2.00	26.96(10)	27.29	2.047
	6	1.06 Mg + 0.79 Al + 0.13 Ti ⁴⁺ + 0.01 V ³⁺ + 0.01 Cr ³⁺	2.00	26.30(10)	26.32	2.016
	7	1.23 Mg + 0.69 Al + 0.08 Ti ⁴⁺	2.00	25.48(11)	25.49	2.026
	8	0.76 Mg + 1.12 Al + 0.08 Ti ⁴⁺ + 0.02 V ³⁺ + 0.02 Cr ³⁺	2.00	26.09(10)	26.38	1.991
M(3)	1	0.79 Mg + 0.17 Al + 0.04 Fe ²⁺	1.00	12.80(6)	12.73	2.057
	2	0.96 Mg + 0.01 Al + 0.03 Fe ²⁺	1.00	12.32(7)	12.43	2.074
	3	0.77 Mg + 0.19 Al + 0.04 Fe ²⁺	1.00	12.36(7)	12.75	2.055
	6	0.93 Mg + 0.05 Al + 0.02 Fe ²⁺	1.00	12.34(7)	12.33	2.070
	7	0.84 Mg + 0.11 Al + 0.05 Fe ²⁺	1.00	12.64(8)	12.81	2.068
	8	0.86 Mg + 0.12 Al + 0.02 Fe ²⁺	1.00	12.27(7)	12.40	2.074
M(4)	1	1.97 Ca + 0.03 Na	2.00	39.69(11)	39.73	2.485
	2	2.00 Ca	2.00	39.97(11)	40.00	2.472
	3	2.00 Ca	2.00	40.41(11)	40.00	2.485
	6	2.00 Ca	2.00	40.60(10)	40.00	2.482
	7	2.00 Ca	2.00	40.38(11)	40.00	2.485
	8	2.00 Ca	2.00	40.15(11)	40.00	2.472
A(m)	1	0.48 Na + 0.06 K	0.54	6.51(2)	6.42	2.555
	2	0.04 Na + 0.28 K	0.32	5.33(2)	5.76	2.611
	3	0.40 Na + 0.05 K	0.45	5.55(3)	5.35	2.589
	6	0.07 Na + 0.44 K	0.51	7.98(3)	9.13	2.631
	7	0.05 Na + 0.42 K	0.47	7.29(3)	8.53	2.633
	8	0.16 Na + 0.18 K	0.34	5.16(3)	5.18	2.589
A(2)	1	0.46 Na	0.46	5.56(2)	5.06	2.646
	2	0.68 Na	0.68	7.09(3)	7.48	2.720
	3	0.55 Na	0.55	5.95(2)	6.05	2.620
	6	0.49 Na	0.49	5.36(2)	5.39	2.767
	7	0.53 Na	0.53	5.82(2)	5.83	2.759
	8	0.66 Na	0.66	7.09(3)	7.26	2.694

bl – bond length

3674 cm⁻¹ decreases with increasing F, further evidence of (OH)–F coupling across the occupied A site. Hawthorne *et al.* (2005) suggested that this coupling is due to differential repulsion between H and the A-site cation, which forces the A cation to occupy a more central position. Where the adjacent O(3) site is occupied by F, no such repulsion occurs and thus the A-group cation moves further away from the OH-group. As a result, the vibrational frequency between the H and A-group cation is reduced, and the OH–^ANa–F arrangement will absorb at a relatively lower wavenumber.

The frequency of local arrangements OH–^ANa–OH, OH–^ANa–F and F–^ANa–F may be calculated from the F content of the crystal (Heavysege *et al.*, 2015) where $x = F/(F + OH)$:

$$\text{OH} - {}^A\text{Na} - \text{OH}: (1 - x)^2 / (1 - x + x^2)$$

$$\text{OH} - {}^A\text{Na} - \text{F}: x(1 - x)^2 / (1 - x + x^2)$$

$$\text{F} - {}^A\text{Na} - \text{F}: x^2 / (1 - x + x^2)$$

The arrangement F–^ANa–F is not visible in the infrared, and the relative intensities for any arrangement involving A = Na (or K) and its F-shifted equivalent may be calculated from the relevant expressions above and the F content of the crystal. Moreover, the relative displacement of the F-shifted equivalent band is ~19 cm⁻¹ (Robert *et al.*, 1999, 2000). Accordingly, the F-shifted MgMgMg–OH–Na:SiAl arrangement should give rise to a band at 3700–3690 cm⁻¹, which is indeed the case (Fig. 5, band B).

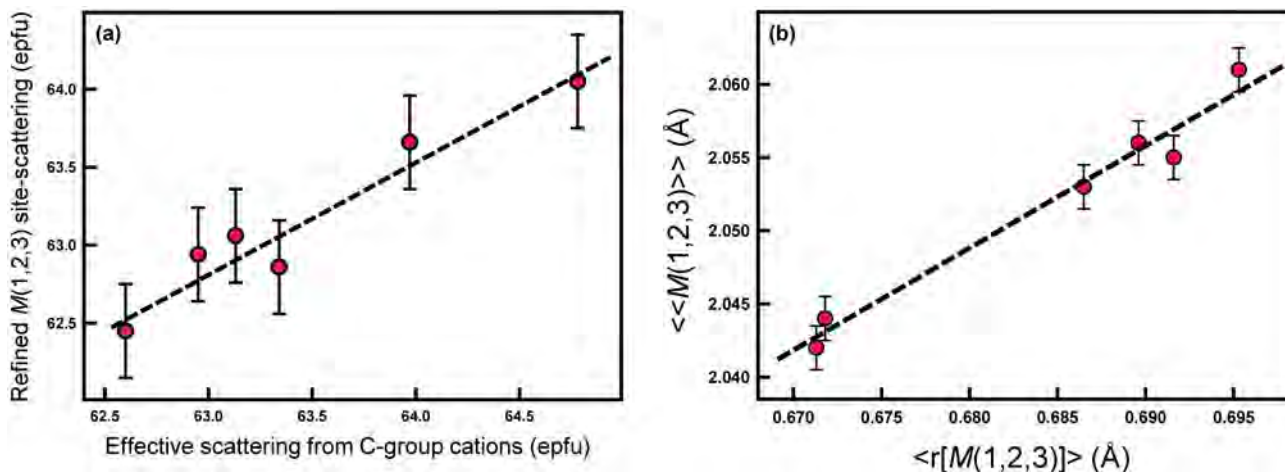


Fig. 3. (a) Effective scattering from C-group cations (epfu) plotted against refined $M(1)$, $M(2)$ and $M(3)$ site-scattering (epfu); (b) mean radius of the $M(1,2,3)$ sites (Å) ($\langle r[M(1,2,3)] \rangle$) plotted against the grand mean $M(1,2,3)$ -O bond lengths (Å) ($\langle \langle r[M(1,2,3)-O] \rangle \rangle$) for each sample (shown as red dots). Dashed black lines represent a linear relation between both variables in (a) and (b).

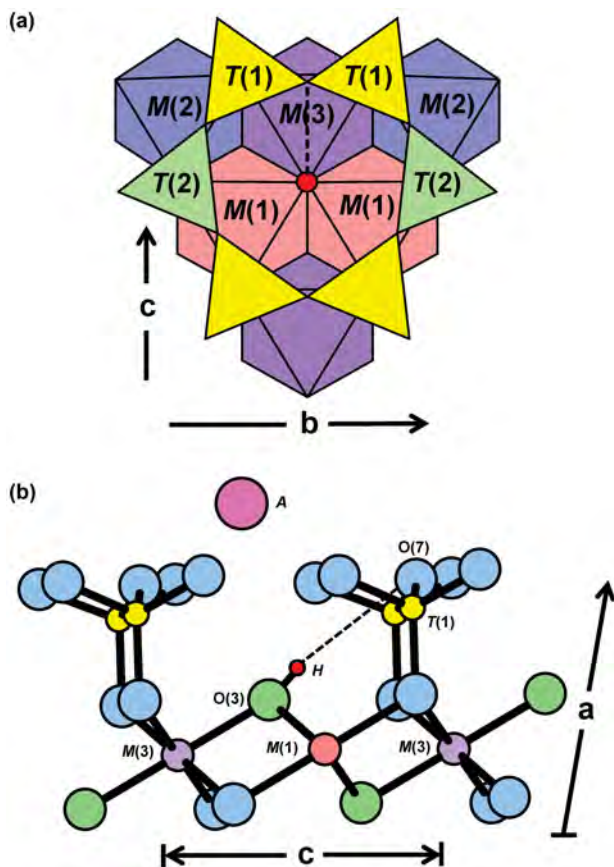


Fig. 4. (a) The local structure surrounding the O(3) site (red circle); (b) connectivity around the O(3) site in $C2/m$ amphiboles projected onto (010). The dashed black line represents the H...O(7) bond in (a) and (b). T(2) sites have been omitted in (b) for simplicity. Modified from Della Ventura *et al.* (1999).

Above in point (2), we saw that the NN configuration has two principal arrangements, MgMgMg and MgMgAl. Hence the arrangements derived above, MgMgMg-OH-Na-OH:SiAl and (F-shifted) MgMgMg-OH-Na-F:SiAl, should have $M(1)M(1)M(3) = \text{MgMgAl}$

equivalents: MgMgAl-OH-Na-OH:SiAl and (F-shifted) MgMgAl-OH-Na-F:SiAl. Thus we expect to see four bands in the infrared spectra of these amphiboles. These MgMgAl-OH-Na-OH:SiAl and MgMgAl-OH-Na-F:SiAl arrangements should give rise to bands at $3687\text{--}3677\text{ cm}^{-1}$ and $3667\text{--}3657\text{ cm}^{-1}$, respectively, as $M(1,3)\text{Mg}$ substituted by $M(1,3)\text{Al}^{3+}$ results in a relative band displacement of -33 cm^{-1} (Della Ventura *et al.*, 1999). Calculating the frequencies of occurrence of these last two arrangements via the relation $\text{MgMgMg}:\text{MgMgAl} = M^{(3)}\text{Mg}^*:M^{(3)}\text{Al}$ ($\text{Mg}^* = \text{Mg} + \text{Fe}^{2+}$) indicates that they are significantly less common than their MgMgMg analogues. However, their absorption is shifted to a lower frequency, and as shown by Skogby and Rossman (1991), the transition probability of absorption increases strongly with decreasing absorption frequency, and hence the ratios of local arrangements do not one-to-one correspond with the absorption intensities of the corresponding bands in the infrared.

Description and interpretation of spectra

The observed band intensities and the amounts of the local arrangements assigned to these bands in the spectra of each amphibole (Fig. 5) are given in Table 6. In general, the observed band intensities and the calculated amounts of the corresponding local arrangements are in reasonable accord. However, the disagreement between observed and calculated values tends to increase among arrangements corresponding to bands at lower frequencies. This is probably due to increased transition probabilities resulting in the lack of one-to-one correspondence between the relative amounts of local arrangements and the intensities of their associated absorption bands (Skogby and Rossman, 1991; Della Ventura *et al.*, 1996a,b; Hawthorne *et al.*, 1997). The results of this effect are apparent for AM2 and AM6. For these crystals, $M^{(3)}\text{Al}$ is low (0.01–0.05 apfu) (Table 5), and one expects the band intensity of any local arrangement involving $M^{(3)}\text{Al}$ (bands C and D) to be relatively low. However, this is not the case as the observed absorption intensities of the bands are significantly higher than predicted (Table 6). The NNN effects of band-splitting, which have been ignored here, could also cause slight discrepancies between band intensities and the calculated amounts of different local arrangements (Della Ventura *et al.*, 1999; Robert *et al.*, 2000).

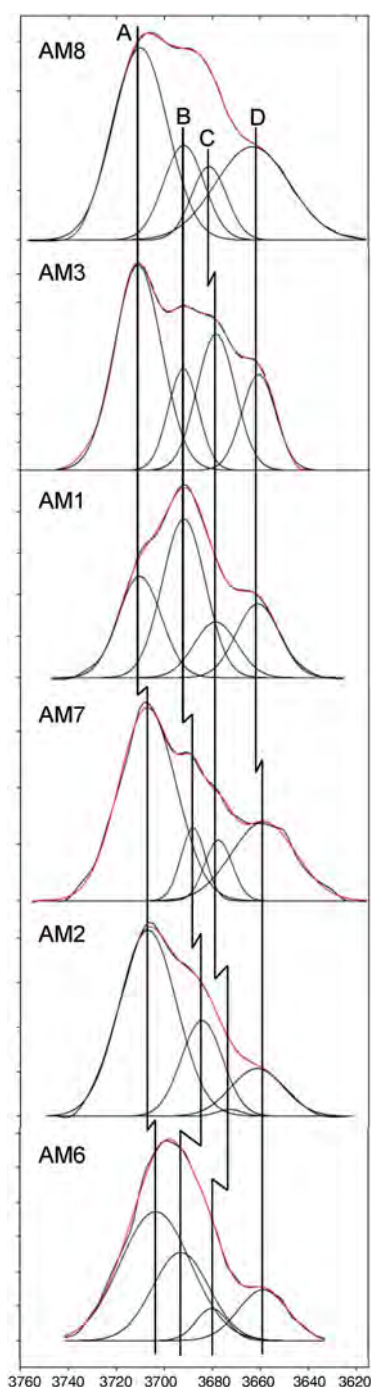


Fig. 5. Comparison of the fitted spectra of each sample in the principal OH-stretching region. Vertical lines represent the peak positions of bands A, B, C and D. Black curves represent the observed spectra and red curves represent the sum of the fitted bands. Note the slight deviations in band centres corresponding to the same local arrangements in each sample.

AM1–3 and 6–8 were each fit using four peaks, corresponding to the local arrangements: (1) MgMgMg–OH–Na–OH:SiAl; (2) MgMgMg–OH–Na–F:SiAl; (3) MgMgAl–OH–Na–OH:SiAl and (4) MgMgAl–OH–Na–F:SiAl (Table 6). Figure 5 shows that most of the observed bands corresponding to the same local arrangement are centred reasonably close to the same wavenumber (cm^{-1}), as one would expect from the arguments proposed previously. However, not all bands corresponding to the same local arrangement are centred at exactly the same wavenumber (cm^{-1})

Table 6. Band positions, band intensities and calculated amounts of the associated local arrangements for gem amphiboles from Mogok, Myanmar.

Band	Centre (cm^{-1})	Band intensity	Calculated amount	Local arrangement
AM1				
A	3709.94	0.27	0.22	MgMgMg–OH–Na–OH: SiAl
B	3691.19	0.43	0.43	MgMgMg–OH–Na–F: SiAl (F-shifted A)
C	3674.90	0.14	0.12	MgMgAl–OH–Na–OH: SiAl
D	3659.93	0.16	0.23	MgMgAl–OH–Na–F: SiAl (F-shifted C)
AM2				
A	3706.91	0.62	0.72	MgMgMg–OH–Na–OH: SiAl
B	3684.46	0.23	0.26	MgMgMg–OH–Na–F: SiAl (F-shifted A)
C	3672.87	0.01	0.015	MgMgAl–OH–Na–OH: SiAl
D	3661.44	0.14	0.005	MgMgAl–OH–Na–F: SiAl (F-shifted C)
AM3				
A	3711.05	0.46	0.56	MgMgMg–OH–Na–OH: SiAl
B	3692.20	0.14	0.17	MgMgMg–OH–Na–F: SiAl (F-shifted A)
C	3678.54	0.25	0.21	MgMgAl–OH–Na–OH: SiAl
D	3660.76	0.15	0.06	MgMgAl–F–Na–OH: SiAl (F-shifted C)
AM6				
A	3703.55	0.52	0.57	MgMgMg–OH–Na–OH: SiAl
B	3693.00	0.28	0.31	MgMgMg–OH–Na–F: SiAl (F-shifted A)
C	3680.07	0.06	0.08	MgMgAl–OH–Na–OH: SiAl
D	3658.74	0.14	0.04	MgMgAl–OH–Na–F: SiAl (F-shifted C)
AM7				
A	3707.18	0.57	0.55	MgMgMg–OH–Na–OH: SiAl
B	3688.12	0.09	0.23	MgMgMg–OH–Na–F: SiAl (F-shifted A)
C	3677.59	0.08	0.15	MgMgAl–OH–Na–OH: SiAl
D	3658.70	0.26	0.07	MgMgAl–OH–Na–F: SiAl (F-shifted C)
AM8				
A	3710.10	0.44	0.60	MgMgMg–OH–Na–OH: SiAl
B	3691.92	0.16	0.21	MgMgMg–OH–Na–F: SiAl (F-shifted A)
C	3681.39	0.11	0.14	MgMgAl–OH–Na–OH: SiAl
D	3663.25	0.29	0.05	MgMgAl–OH–Na–F: SiAl (F-shifted C)

in all samples. For example, Fig. 5 shows that band A is centred at $\sim 3707 \pm 4 \text{ cm}^{-1}$ in all samples; however, it is tightly centred at $\sim 3710 \text{ cm}^{-1}$ in AM1, 3 and 8, and at $\sim 3707 \text{ cm}^{-1}$ in AM2 and 7. A similar correlation is observed for band B, which is tightly centred at $\sim 3692 \text{ cm}^{-1}$ in AM1, 3, 8 and 6 and at $\sim 3684 \text{ cm}^{-1}$ and $\sim 3688 \text{ cm}^{-1}$ in AM2 and 7, respectively (Table 6).

Most of the curves used to fit the observed spectra have band centres that fall well within the theoretical frequency ranges calculated previously. Nonetheless, certain chemical features may explain minor differences in band position. $^{M(1,3)}\text{Fe}^{2+}$ ranges from 0.02–0.12 apfu (Table 5) and results in a frequency shift of -15 to -18 cm^{-1} where substituting for $^{M(1,3)}\text{Mg}$, only half the frequency shift produced by $^{M(1,3)}\text{Mg} \leftrightarrow ^{M(1,3)}\text{Al}$ (-33 cm^{-1}) (Iezzi *et al.*, 2005; Della Ventura *et al.*, 1999). Even though the relatively low amount of Fe^{2+} may have discernible effects in the infrared, it is probably masked by the MgMgMg–OH–Na–F:SiAl arrangement ($\sim 3692 \text{ cm}^{-1}$) as the arrangement MgMgMg–OH–Na–OH:SiAl may be shifted -15 to -18 cm^{-1} via the substitution $^{M(1,3)}\text{Mg} \leftrightarrow ^{M(1,3)}\text{Fe}^{2+}$, from 3711 cm^{-1} to 3693 – 3696 cm^{-1} . The amount of ^AK in most samples is significant and ranges from 0.05–0.44 apfu (Table 5). Although all local arrangements are written with Na as the A-site constituents, K partly occupies the A site in all samples and may account for some minor differences in band position between samples as $^A\text{Na} \leftrightarrow ^A\text{K}$ results in a frequency shift of $+5 \text{ cm}^{-1}$ (Robert *et al.*, 1989).

Summary

In all samples, ^TAl occupies both $T(1)$ and $T(2)$ but is strongly ordered at $T(1)$. $M(1,2,3)$ are dominated by $^{[6]}\text{Mg}$, $^{[6]}\text{Al}$ is partly

disordered over $M(2)$ and $M(3)$ and is absent at $M(1)$. $^{61}\text{Fe}^{2+}$ is disordered over $M(1,2,3)$ and minor trivalent and tetravalent cations (Cr^{3+} , V^{3+} and Ti^{4+}) are weakly ordered at $M(2)$. $M(4)$ is completely occupied by Ca, except for AM1 which contains minor $^{M(4)}\text{Na}$. $A(2)$ is dominated by Na and $A(m)$ is occupied by both Na and K (Table 5). The $^{O(3)}(\text{OH})\text{:F}$ ratio ranges from 1.42:0.58 (AM3) to 0.84:1.16 (AM6) (Table 4).

Band A at $\sim 3707\text{ cm}^{-1}$ is the most intense (Fig. 5) and corresponds to the local arrangement $\text{MgMgMg-OH-Na-OH:SiAl}$. Band B at $\sim 3692\text{ cm}^{-1}$ is typically the second most intense band and corresponds to the arrangement $\text{MgMgMg-OH-Na-F:SiAl}$, the F-shifted equivalent of band A. Bands C and D correspond to the arrangements $\text{MgMgAl-OH-Na-OH:SiAl}$ and $\text{MgMgAl-OH-Na-F:SiAl}$, respectively. There is reasonable agreement between observed band intensities and calculated ratios of the corresponding arrangements (Table 6), supporting the assignment of these bands to these specific local arrangements.

Acknowledgements. This work was supported by a Discovery Grant from the Natural Sciences and Engineering Research Council of Canada to FCH, and by Innovation Grants from the Canada Foundation for Innovation to FCH. We would like to thank Dudley Blowett of Mountain Minerals, Colorado for supplying some sample material.

Supplementary material. To view supplementary material for this article, please visit <https://doi.org/10.1180/mgm.2018.149>

References

- Abdu Y. and Hawthorne F.C. (2009) Crystal structure and Mössbauer spectroscopy of tschermakite from the ruby locality at Fiskenaeset, Greenland. *The Canadian Mineralogist*, **47**, 917–926.
- Bocchio R., Ungaretti L. and Rossi G. (1978) Crystal chemical study of eclogitic amphiboles from Alpe Arami, Lepontine Alps, Southern Switzerland. *Rendiconti della Società Italiana di Mineralogia e Petrologia*, **34**, 453–470.
- Boschmann K., Burns P.C., Hawthorne F.C., Raudsepp M. and Turnock A.C. (1994) A-site disorder in synthetic fluor-edenite, a crystal structure study. *The Canadian Mineralogist*, **47**, 21–30.
- Chang I.F. and Mitra S.S. (1968) Application of a modified random-element-isodisplacement model to long-wavelength optic phonons of mixed crystals. *Physical Review*, **172**, 924–933.
- Della Ventura G., Robert J.-L. and Hawthorne F.C. (1996a) Infrared spectroscopy of synthetic (Ni,Mg,Co)-potassium-richterite. Pp. 55–63 in: *Mineral Spectroscopy: A Tribute to Roger G. Burns* (M.D. Dyar, C. McCammon and M.W. Schaefer, editors). The Geochemical Society Special Publication **No. 5**. The Geochemical Society, Washington, DC.
- Della Ventura G., Robert J.-L., Hawthorne F.C. and Prost R. (1996b) Short-range disorder of Si and Ti in the tetrahedral double-chain unit of synthetic Ti-bearing potassium-richterite. *American Mineralogist*, **81**, 56–60.
- Della Ventura G., Robert J.-L., Raudsepp M., Hawthorne F.C. and Welch M.D. (1997) Site occupancies in synthetic monoclinic amphiboles: Rietveld structure-refinement and infrared spectroscopy of (nickel, magnesium, cobalt)-richterite. *American Mineralogist*, **82**, 291–301.
- Della Ventura G., Robert J.-L. and Hawthorne F.C. (1998a) Characterization of OH-F short-range order in potassium-fluor-richterite by infrared spectroscopy in the OH-stretching region. *The Canadian Mineralogist*, **36**, 181–185.
- Della Ventura G., Robert J.-L., Hawthorne F.C., Raudsepp M. and Welch M.D. (1998b) Contrasting patterns of ^{61}Al order in synthetic pargasite and Co-substituted pargasite. *The Canadian Mineralogist*, **36**, 1237–1244.
- Della Ventura G., Hawthorne F.C., Robert J.-L., Delbove F., Welch M.F. and Raudsepp M. (1999) Short-range order of cations in synthetic amphiboles along the richterite-pargasite join. *European Journal of Mineralogy*, **11**, 79–94.
- Della Ventura G., Robert J.-L., Sergent J., Hawthorne F.C. and Delbove F. (2001) Constraints on F vs. OH incorporation in synthetic ^{61}Al -bearing in monoclinic amphiboles. *European Journal of Mineralogy*, **13**, 841–847.
- Della Ventura G., Hawthorne F.C., Robert J.-L. and Iezzi G. (2003) Synthesis and infrared spectroscopy of amphiboles along the tremolite-pargasite join. *European Journal of Mineralogy*, **15**, 341–347.
- Della Ventura G., Oberti R., Hawthorne F.C. and Bellatreccia F. (2007) FTIR spectroscopy of Ti-rich pargasites from Lherz and the detection of $\text{O}^{2\text{B}}$ at the anionic O3 site in amphiboles. *American Mineralogist*, **92**, 1645–1651.
- Della Ventura G., Bellatreccia F., Cámara F. and Oberti R. (2014) Crystal-chemistry and short-range order of fluoroedenite and fluoro-pargasite: a combined X-ray diffraction and FTIR spectroscopic approach. *Mineralogical Magazine*, **78**, 293–310.
- Gottschalk M., Andrut M. and Melzer S. (1999) The determination of cummingtonite content of synthetic tremolite. *European Journal of Mineralogy*, **11**, 967–982.
- Hawthorne F.C. (1981) Crystal chemistry of the amphiboles. Pp. 1–102 in: *Amphiboles and Other Hydrous Pyriboles: Mineralogy* (David R. Veblen and Paul H. Ribbe, editors). Reviews in Mineralogy, **9A**. Mineralogical Society of America, Washington, DC.
- Hawthorne F.C. (1983a) The crystal chemistry of the amphiboles. *The Canadian Mineralogist*, **21**, 173–480.
- Hawthorne F.C. (1983b) Characterization of the average structure of natural and synthetic amphiboles. *Periodico di Mineralogia*, **52**, 543–581.
- Hawthorne F.C. (1983c) Quantitative characterization of site occupancies in minerals. *American Mineralogist*, **68**, 287–306.
- Hawthorne F.C. (1997) Short-range order in amphiboles: a bond-valence approach. *The Canadian Mineralogist*, **35**, 203–218.
- Hawthorne F.C. (2016) Short-range atomic arrangements in minerals. I: The minerals of the amphibole, tourmaline and pyroxene supergroups. *European Journal of Mineralogy*, **28**, 513–536.
- Hawthorne F.C. and Della Ventura G. (2007) Short-range order in amphiboles. Pp. 173–222 in: *Amphiboles: Crystal Chemistry, Occurrence, and Health Issues* (Frank C. Hawthorne, Roberta Oberti, Giancarlo Della Ventura and Annibale Mottana, editors). Reviews in Mineralogy & Geochemistry, **67**. The Mineralogical Society of America and the Geochemical Society, Chantilly, Virginia, USA.
- Hawthorne F.C. and Grundy H.D. (1972) Positional disorder in the A-site of clino-amphiboles. *Nature*, **235**, 72.
- Hawthorne F.C. and Grundy H.D. (1973a) The crystal chemistry of the amphiboles. I. Refinement of the crystal structure of ferrotschermakite. *Mineralogical Magazine*, **39**, 36–48.
- Hawthorne F.C. and Grundy H.D. (1973b) The crystal chemistry of the amphiboles. II. Refinement of the crystal structure of oxykaersutite. *Mineralogical Magazine*, **39**, 390–400.
- Hawthorne F.C. and Grundy H.D. (1976) The crystal chemistry of the amphiboles. IV. X-ray and neutron refinements of the crystal structure of tremolite. *The Canadian Mineralogist*, **14**, 334–345.
- Hawthorne F.C. and Grundy H.D. (1977) The crystal chemistry of the amphiboles. III. Refinement of the crystal structure of a sub-silicic hastingsite. *Mineralogical Magazine*, **41**, 43–50.
- Hawthorne F.C. and Oberti R. (2007) Amphiboles: crystal chemistry. pp. 1–54 in: *Amphiboles: Crystal Chemistry, Occurrence, and Health Issues* (Frank C. Hawthorne, Roberta Oberti, Giancarlo Della Ventura and Annibale Mottana, editors). Reviews in Mineralogy & Geochemistry, **67**. The Mineralogical Society of America and the Geochemical Society, Chantilly, Virginia, USA.
- Hawthorne F.C., Ungaretti L. and Oberti R. (1995) Site populations in minerals: terminology and presentation of results of crystal-structure refinement. *The Canadian Mineralogist*, **33**, 907–911.
- Hawthorne F.C., Della Ventura G. and Robert J.-L. (1996a) Short-range order of (Na, K) and Al in tremolite: An infrared study. *American Mineralogist*, **81**, 782–784.
- Hawthorne F.C., Oberti R. and Sardone N. (1996b) Sodium at the A site in clinoamphiboles: the effects of composition on patterns of order. *The Canadian Mineralogist*, **34**, 577–593.
- Hawthorne F.C., Della Ventura G., Robert J.-L., Welch M.F., Raudsepp M. and Jenkins D.M. (1997) A Rietveld and infrared study of synthetic amphiboles along the potassium-richterite-tremolite join. *American Mineralogist*, **82**, 708–716.
- Hawthorne F.C., Welch M.D., Della Ventura G., Liu S., Robert J.-L. and Jenkins D.M. (2000) Short-range order in synthetic aluminous tremolites:

- An infrared and triple-quantum MAS NMR study. *American Mineralogist*, **85**, 1716–1724.
- Hawthorne F.C., Della Ventura G., Oberti R., Robert J.-L. and Iezzi G. (2005) Short-range order in minerals: amphiboles. *The Canadian Mineralogist*, **43**, 1895–1920.
- Hawthorne F.C., Oberti R., Harlow G.E., Maresch W., Martin R.F., Schumacher J.C. and Welch M.D. (2012) Nomenclature of the amphibole super-group. *American Mineralogist*, **97**, 2031–2048.
- Heavyside D., Abdu Y. and Hawthorne F.C. (2015) Long-range and short-range order in gem pargasite from Myanmar: Crystal structure refinements and infrared spectroscopy. *The Canadian Mineralogist*, **53**, 497–510.
- Iezzi G., Della Ventura G., Hawthorne F.C., Pedrazzi G. and Robert J.-L. (2005) The (Mg,Fe²⁺) substitution in ferri-clinoholmquistite, □Li₂(Mg,Fe²⁺)₃Fe³⁺Si⁴⁺O₂₂(OH)₂. *European Journal of Mineralogy*, **17**, 733–740.
- Jenkins D.M. (1987) Synthesis and characterization of tremolite in the system H₂O–CaO–MgO–SiO₂. *American Mineralogist*, **72**, 707–715.
- Jenkins D.M., Sherriff B.L., Cramer J. and Xu Z. (1997) Al, Si and Mg occupancies in tetrahedrally and octahedrally coordinated sites in synthetic aluminous tremolite. *American Mineralogist*, **82**, 280–290.
- Leissner L., Schlüter J., Horn I. and Mihailova B. (2015) Exploring the potential of Raman spectroscopy for crystallochemical analyses of complex hydrous silicates: I. Amphiboles. *American Mineralogist*, **100**, 2682–2694.
- Najorka J. and Gottschalk M. (2003) Crystal chemistry of tremolite-tschermakite solid solutions. *Physics and Chemistry of Minerals*, **30**, 108–124.
- Oberti R., Ungaretti L., Cannillo E., Hawthorne F.C. and Memmi I. (1995a) Temperature-dependent Al order-disorder in the tetrahedral double-chain of C2/m amphiboles. *European Journal of Mineralogy*, **7**, 1049–1063.
- Oberti R., Hawthorne F.C., Ungaretti L. and Cannillo E. (1995b) ⁶Al disorder in amphiboles from mantle peridotites. *The Canadian Mineralogist*, **33**, 867–878.
- Oberti R., Sardone N., Hawthorne F.C., Raudsepp M. and Turnock A.C. (1995c) Synthesis and crystal-structure refinement of synthetic fluor-pargasite. *The Canadian Mineralogist*, **33**, 25–31.
- Oberti R., Hawthorne F.C., Cámara F. and Raudsepp M. (1998) Synthetic fluoro-amphiboles: site preferences of Al, Ga, Sc and inductive effects on mean bond-lengths of octahedra. *The Canadian Mineralogist*, **36**, 1245–1252.
- Oberti R., Hawthorne F.C., Cannillo E. and Cámara F. (2007) Long-range order in amphiboles. Pp. 125–171 in: *Amphiboles: Crystal Chemistry, Occurrence, and Health Issues* (Frank C. Hawthorne, Roberta Oberti, Giancarlo Della Ventura and Annibale Mottana, editors). Reviews in Mineralogy & Geochemistry, **67**. The Mineralogical Society of America and the Geochemical Society, Chantilly, Virginia, USA.
- Papike J.J., Ross M. and Clark J.R. (1969) Crystal-chemical characterization of clin amphiboles based on five new structure refinements. *Mineralogical Society of America Special Paper*, **2**, 117–136.
- Pouchou J.L. and Pichoir F. (1985) 'PAP' (φρZ) procedure for improved quantitative microanalysis. Pp. 104–106 in: *Microbeam Analysis* (J.T. Armstrong, editor). San Francisco Press, San Francisco, California, USA.
- Raudsepp M., Turnock A.C. and Hawthorne F.C. (1987a) Characterization of cation ordering in synthetic scandium-fluor-eckermannite, indium-fluor-eckermannite and scandium-fluor-nyböite by Rietveld structure refinement. *American Mineralogist*, **72**, 959–964.
- Raudsepp M., Turnock A.C., Hawthorne F.C., Sherriff B.L. and Hartman J.S. (1987b) Characterization of synthetic pargasitic amphiboles (NaCa₂Mg₄M³⁺Si₆Al₂O₂₂(OH,F)₂; M³⁺ = Al, Cr, Ga, Sc, In) by infrared spectroscopy, Rietveld structure refinement and ²⁷Al, ²⁹Si, and ¹⁹F MAS NMR spectroscopy. *American Mineralogist*, **72**, 580–593.
- Raudsepp M., Turnock A.C. and Hawthorne F.C. (1991) Amphiboles synthesis at low-pressure: what grows and what doesn't. *European Journal of Mineralogy*, **3**, 983–1004.
- Robert J.-L., Della Ventura G. and Thauvin J.-L. (1989) The infrared OH-stretching region of synthetic richterites in the system Na₂O–K₂O–CaO–MgO–SiO₂–H₂O–HF. *European Journal of Mineralogy*, **1**, 203–211.
- Robert J.-L., Della Ventura G. and Hawthorne F.C. (1999) Near-infrared study of short-range disorder of OH and F in monoclinic amphiboles. *American Mineralogist*, **84**, 86–91.
- Robert J.-L., Della Ventura G., Welch M.D. and Hawthorne F.C. (2000) The OH/F substitution in synthetic pargasite at 1.5kbar, 850°C. *American Mineralogist*, **85**, 926–931.
- Robinson K., Gibbs G.V., Ribbe P.H. and Hall M.R. (1973) Cation distributions in three hornblendes. *American Journal of Science*, **273A**, 522–535.
- Semet M.P. (1973) A crystal-chemical study of synthetic magnesiohastingsite. *American Mineralogist*, **58**, 480–494.
- Shannon R.D. (1976) Revised effective ionic radii and systematic studies of interatomic distances in halides and chalcogenides. *Acta Crystallographica*, **A32**, 751–767.
- Sheldrick G.M. (2008) A short history of SHELX. *Acta Crystallographica*, **A64**, 112–122.
- Skogby H. and Rossman G.R. (1991) The intensity of amphibole OH bands in the infrared absorption spectrum. *Physics and Chemistry of Minerals*, **18**, 64–68.
- Strens R.G.J. (1966) Infrared study of cation ordering and clustering in some (Fe,Mg) amphibole solid solutions. *Chemical Communications (Chemical Society of London)*, **15**, 519–520.
- Tait K.T., Hawthorne F.C. and Della Ventura G. (2001) Al-Mg disorder in a gem-quality pargasite from Baffin Island, Nunavut, Canada. *The Canadian Mineralogist*, **39**, 1725–1732.
- Welch M.D. and Knight K.S. (1999) A neutron powder diffraction study of cation ordering in high-temperature synthetic amphiboles. *European Journal of Mineralogy*, **11**, 321–331.
- Welch M.D., Kolodziejewski W. and Klinowski J. (1994) A multinuclear study of synthetic pargasite. *American Mineralogist*, **79**, 261–268.
- Welch M.D., Liu S. and Klinowski J. (1998) ²⁹Si MAS NMR systematics of calcic and sodic-calcic amphiboles. *American Mineralogist*, **83**, 85–96.
- Wojdyr M. (2010) Fityk: a general-purpose peak fitting program. *Journal of Applied Crystallography*, **43**, 1126–1128.